IEEE Photonics Journal
An IEEE Photonics Society Publication

Open Access

Indium Tin Oxide Coated Two-Mode Fiber for Enhanced SPR Sensor in Near-Infrared Region

Volume 9, Number 6, December 2017

Yajun Wang
Jiangli Dong
Yunhan Luo
Jieyuan Tang
Huihui Lu
Jianhui Yu
Heyuan Guan
Jun Zhang
Zhe Chen

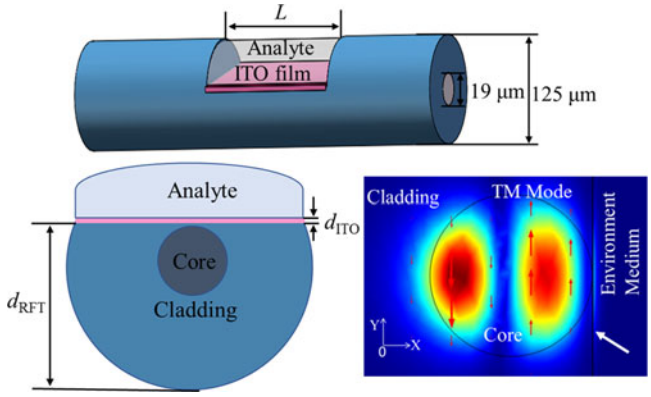

DOI: 10.1109/JPHOT.2017.2757513
1943-0655 © 2017 IEEE

IEEE photonics SOCIETY

IEEE

Indium Tin Oxide Coated Two-Mode Fiber for Enhanced SPR Sensor in Near-Infrared Region

Yajun Wang,[1,2] Jiangli Dong,[1,2] Yunhan Luo,[1,2,3] Jieyuan Tang,[3,4] Huihui Lu,[1,4] Jianhui Yu,[1,4] Heyuan Guan,[1,3] Jun Zhang,[4] and Zhe Chen[3,4]

[1]Guangdong Provincial Key Laboratory of Optical Fiber Sensing and Communications, Jinan University, Guangzhou 510632, China
[2]Department of Optoelectronic Engineering, Jinan University, Guangzhou 510632, China
[3]Key Laboratory of Optoelectronic Information and Sensing Technologies of Guangdong Higher Education Institutes, Jinan University, Guangzhou 510632, China
[4]Key Laboratory of Visible Light Communications of Guangzhou, Jinan University, Guangzhou 510632, China

DOI:10.1109/JPHOT.2017.2757513

Manuscript received August 9, 2017; revised September 18, 2017; accepted September 25, 2017. Date of publication October 11, 2017; date of current version October 23, 2017. This work was supported in part by the National Natural Science Foundation of China (61575084, 61705087, 61361166006, 61401176, 61405075, 61475066, and 61505069), in part by the Natural Science Foundation of Guangdong Province (2015A030313320, S2013050014606, 2014A030313377, 2014A030310205, 2015A030306046, 2016A030311019, 2016A030313079, and 2016A030310098), in part by the Science and Technology Projects of Guangdong Province (2017A010101013, 2012A032300016, 2014B010120002, 2014B010117002, 2015A020213006, 2015B010125007, 2016B010111003, and 2016A010101017), in part by the Science and Technology Project of Guangzhou (201707010500, 201506010046, 201607010134, 201605030002, 201610010026, and 201604040005). Corresponding authors: Jiangli Dong and Yunhan Luo (e-mail: jldong@jnu.edu.cn; yunhanluo@163.com).

Abstract: A surface plasmon resonance (SPR) sensor based on side-polished two-mode fiber (TMF) coated with indium tin oxide (ITO) film is proposed. ITO enables tuning of resonance wavelength of the sensor through changing its carrier concentration. The advantages of the TMF and ITO are combined in the sensor, which can achieve high sensitivity and plasma frequencies in the near-infrared region. The impact of ITO film thickness and residual fiber thickness on the sensing performance are numerically investigated with LP_{01} and LP_{11a} modes coupled to specific surface plasmon modes. The results show that the resonance wavelength locates in 1500–2200 nm and an average sensitivity of ~10149 and ~10400 nm/RIU can be achieved for LP_{01} and LP_{11a} modes, respectively, when the environmental refractive index varies between 1.33 and 1.39. The penetration depths of evanescent wave for the LP_{01} and LP_{11a} modes are 460 and 502 nm, respectively. Both the sensitivity and penetration depth of the sensor are larger than those of single-mode fiber and multimode fiber based SPR sensors. The proposed sensor can play an important role in various applications, including environment, medicine, and security.

Index Terms: Surface plasmon, two-mode fiber, fiber optics sensors, near infrared.

1. Introduction

Surface plasmon resonance (SPR) occurs at a particular wavelength when the phase matching between the light and the surface plasmon (SP) wave is satisfied. The resonant wavelength is

sensitive to the refractive index of the surrounding medium, which is applied in sensing of chemical, environmental and biological fields [1]–[3]. The fiber-based SPR sensors have many advantages compared with the prism-based SPR sensors, such as easy for alignment, online measurement, miniaturized probe and remote sensing [4]–[6]. The performance of the sensor relies on interactions between the evanescent fields escaped through the fiber cladding and the surrounding medium. Many sensor configurations have been proposed to enhance the evanescent field, ranging from chemically etched fibers [7], to side-polished fibers [8], [9], D-shaped fibers [10], tapered fibers [11], hetero-core structures [12], bent fiber probes [13]. Among these fiber configurations, the side-polished fiber is simple in fabrication, and its planar surface provides an ideal platform for film deposition.

In order to improve the sensing performance of SPR sensors, it is important to develop the fiber architectures and plasmonic coatings [14]. Various fiber architectures have been proposed for realizing miniaturized SPR sensors, including single-mode fiber (SMF) [15], [16], multimode fiber (MMF) [17], [18], photonic crystal fiber (PCF) [19]–[23], polarization maintaining fiber (PMF) [24], and multiple-core fiber SPR sensors [25]. SPR sensors based on SMF have been reported with a typical sensitivity of 3150 nm/RIU [24]. MMFs are commonly used to construct the SPR sensor because fabrication of the sensor is relatively simple. An SPR sensor based on MMF with a sensitivity of 4989 nm/RIU was demonstrated [17]. However, the large number of modes in the MMF can excite many SP modes, which results in a broadened linewidth of the SPR spectrum and hence cause reduced sensing performance. In order to overcome this limitation, reducing the number of guided modes that are phase matched with the SP modes is required. This can be realized by using few-mode fiber (FMF) for constructing the SPR sensor, where only several guided modes satisfy the resonant condition. The FMF is able to generate narrower linewidth of the SPR spectrum than the MMF. In addition, the FMF is much easier for fiber processing such as side-polishing and tapering in comparison with the SMF [26].

On the other hand, plasmonic coatings have important effect on the sensing performance. Generally, aluminum (Al), copper (Cu), gold (Au), and silver (Ag) are coated on the fiber for SPR sensor applications. Although Ag provides narrow spectral width, the Ag-based sensor is vulnerable to oxidation which limits its sensing applications such as refractive index sensor [27]. In addition, thin layers of Au cause islands and intraband transitions in the visible range [28]. Moreover, the Cu-based sensor gets oxidized quickly and it is vulnerable to corrosion, which limits the sensitivity and accuracy in sensing applications. These metal materials provide resonance wavelengths that locate in the visible wavelength region. SPR sensors that have plasma frequencies in near-infrared (NIR) region are required in chemical and biomedical applications [29], [30]. For example, an SPR sensor operating in the NIR has been developed for real time monitoring the dynamic processes of living cells [29]. This SPR sensor provides a penetration depth of $\sim 2\,\mu$m, which is much larger than the probe depth of the SPR sensor in the visible wavelength ($\sim$200–300 nm). The SPR sensors in the NIR offer several advantages for sensing. Firstly, the evanescent wave in NIR can penetrate deep into the analyte, indicating higher sensitivity. Secondly, photodamage and phototoxicity to the living materials can be avoided using sensors in the NIR. Thirdly, the fiber-based SPR sensor in NIR has lower loss because the fiber transmission loss in this region is much lower. Graphene has been used to enhance the sensitivity for gas sensing in the NIR [31], [32]. In order to construct SPR sensors operate in the NIR, indium tin oxide (ITO) has been used as the plasmonic coating [20], [21], [33], [34]. The resonance wavelength of the sensor can be tuned by changing the carrier concentration of ITO [30], [35]. ITO provides certain advantages in comparison with the typical metal materials. ITO has large dielectric constant that can improve the sensitivity of the sensor. It was reported that the ITO-coated SPR sensor is $\sim$ 60% more sensitive in comparison with the gold-coated SPR sensors [34]. In addition, islands and intraband transitions can be avoided using the ITO thin film. Moreover, ITO is able to react with different kinds of gases and chemicals, which can be applied for detection of various materials.

In this paper, we propose and numerically investigate an SPR sensor based on a side-polished two-mode fiber (TMF) coated with ITO. For enhancing the evanescent field and improving the sensitivity of the sensor, the TMF fiber with a D-shaped configuration is adopted. The TMF is easy

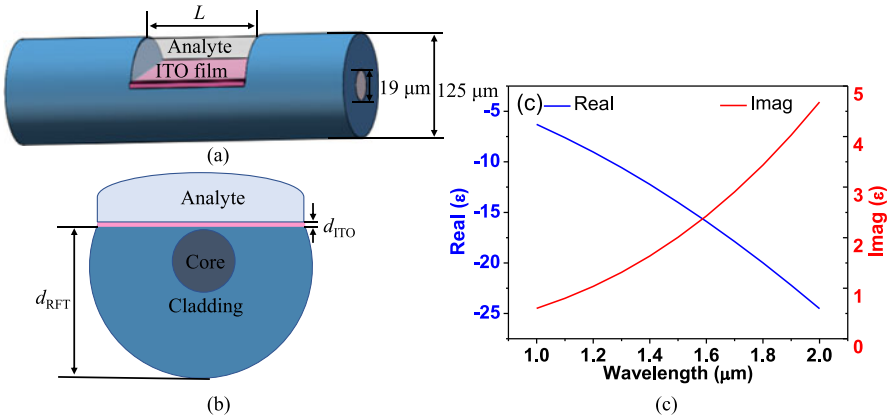

Fig. 1. (a) Schematic of the side-polished SPR sensor. (b) Cross section of the sensor. (c) The real and imaginary parts of the ITO permittivity.

for fiber processing. In addition, the ITO based sensor can operate in the NIR taking advantage of its tunable refractive index. The advantages of the TMF and ITO are combined to improve the sensing performance. The sensor can achieve high sensitivity and large penetration depth in the NIR. The effects of ITO film thickness and residual fiber thickness on the sensing performance are investigated.

2. Simulation Model

The proposed SPR sensor is shown in Fig. 1(a), and the cross section of the sensor is shown in Fig. 1(b). A portion of cladding of TMF is removed to form a D-shaped structure. The flat surface of the side-polished fiber allows coating of ITO film, which provides an ideal platform for interaction between evanescent wave and the analyte. The software COMSOL Multiphysics based on finite element method is used to numerically calculate the electric field intensity and the effective index of mode along the transverse plane of the side-polished fiber. The main design parameters are length of the sensor ($L = 3$ mm), radiuses of the core and cladding (9.5 μm and 62.5 μm, respectively), refractive indices of core and cladding (1.449 and 1.444, respectively), residual fiber thickness d_{RFT}, ITO film thickness d_{ITO}, and refractive index of the environment medium n_e. The permittivity of ITO can be tuned by varying the carrier concentration, which can be described by the Drude-Lorentz model [36]. Both the resonance wavelength and sensing performance of the sensor depend on the permittivity of ITO. The carrier concentration of ITO is chosen to be 2.48×10^{21} cm^{-3} for tuning the sensor operation wavelength to NIR. Fig. 1(c) shows the real and imaginary parts of the ITO permittivity in the wavelength range from 1.0 to 2.0 μm. The real part of the permittivity is negative, while the imaginary part is positive, and there is a crossing point near 1.6 μm.

3. Results and Discussions

3.1 Optimization of the Sensor

Firstly, dispersion properties of the core modes LP_{01}, LP_{11a}, LP_{11b}, LP_{21a}, LP_{21b} are analyzed, with $d_{ITO} = 150$ nm, $d_{RFT} = 72$ μm, $n_e = 1.34$. Fig. 2(a) and (b) show the real and imaginary parts of effective indices of the TM core modes as a function of wavelength, respectively. The real parts of effective indices for different modes decrease with wavelength ranging from 1.3 to 2.0 μm. The imaginary parts of effective indices reach their peaks near 1.6 μm, which are the SPR resonance wavelengths for different modes. As shown in Fig. 2(b), the maxima values of the imaginary parts are different for different modes, and the LP_{11a} mode has the largest value. The SPR resonance is characterized by the peak of the imaginary part of effective index, where the phase matching for coupling between the core mode and SP mode is achieved. The resonance wavelength is

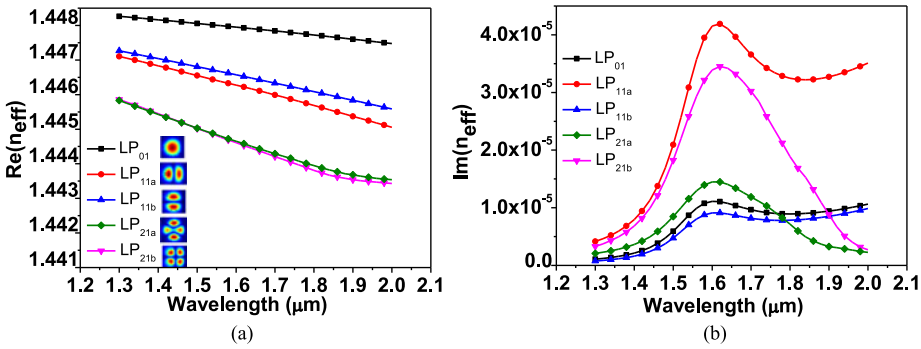

Fig. 2. Dispersion properties of TM core modes with $d_{ITO} = 150$ nm, $d_{RFT} = 72\ \mu$m and $n_e = 1.34$. (a) Real parts of effective indices for the modes LP_{01}, LP_{11a}, LP_{11b}, LP_{21a}, LP_{21b}. (b) Imaginary parts of effective indices for the modes LP_{01}, LP_{11a}, LP_{11b}, LP_{21a}, LP_{21b}.

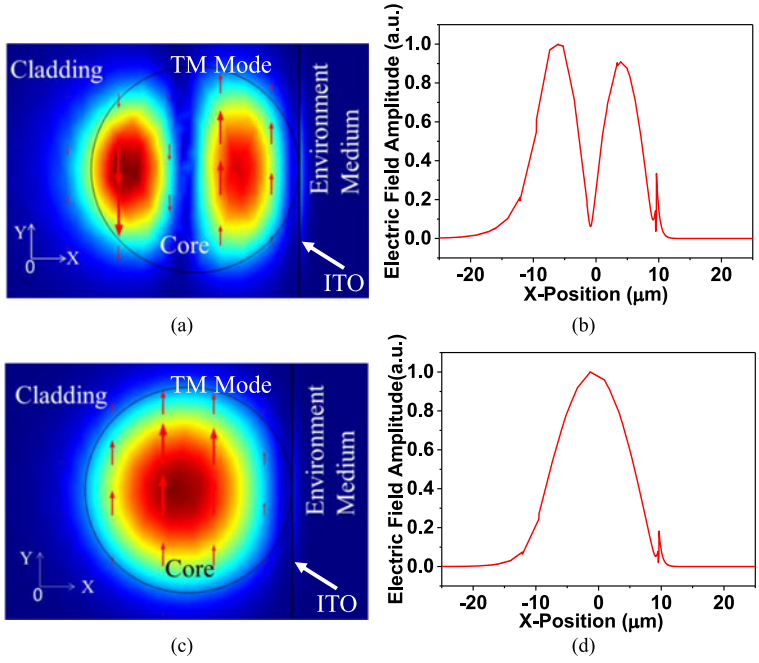

Fig. 3. (a) Electric field intensity for coupling between the LP_{11a} mode and an SP mode and (b) the corresponding 1D electrical field amplitude. (c) Electric field intensity for coupling between the LP_{01} mode and an SP mode and (d) the corresponding 1D electrical field amplitude.

considered for investigating the dependence of sensing performance on the ITO film thickness and residual fiber thickness.

Next, we focus on the LP_{01} and LP_{11a} modes in investigating the sensing performance as they can be selectively excited in the TMF. In order to verify the SPR, the electric field distributions of the D-shape section with $d_{ITO} = 150$ nm, $d_{RFT} = 72\ \mu$m and $n_e = 1.34$ are plotted in Fig. 3. Fig. 3(a) illustrates the electric field intensity for coupling between the LP_{11a} mode and an SP mode at the resonant wavelength of 1609 nm, where the arrows specify the orientation of electric field. The corresponding 1D electrical field amplitude in the optical fiber is shown in Fig. 3(b). As shown in Fig. 3(b), at $X = 9.64\ \mu$m, corresponding to the plane of the ITO film, a sharp peak in the electrical field amplitude is apparent, indicating the existing of SPR. The electric field distribution at the surface of the ITO film in Fig. 3(a) corresponds to the peak of the 1D electrical field amplitude at $X = 9.64\ \mu$m in Fig. 3(b). Fig. 3(c) plots the electric field intensity for coupling between the LP_{01} mode and an SP mode at the resonant wavelength of 1598 nm, the corresponding 1D electrical

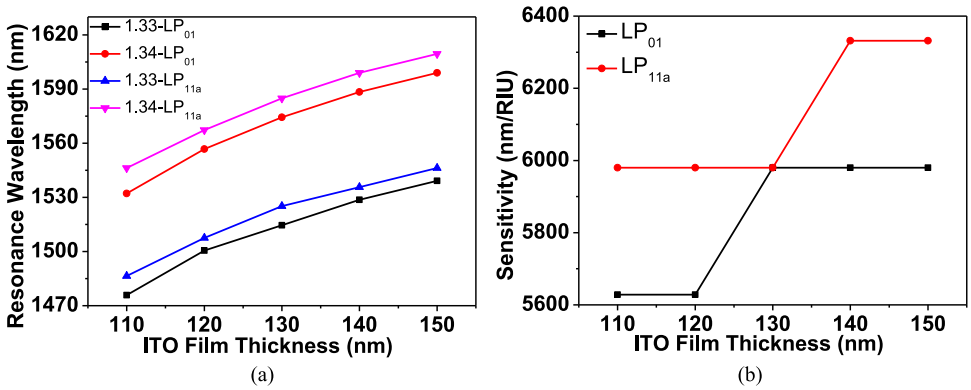

Fig. 4. (a) Dependence of resonant wavelength on ITO film thickness with $d_{RFT} = 72\,\mu$m and n_e varied from 1.33 to 1.34. (b) Sensitivity variation with ITO film thickness for LP_{01} and LP_{11a} modes with n_e increased from 1.33 to 1.34.

field amplitude is shown in Fig. 3(d). Note that the evanescent filed of the LP_{11a} mode is larger than that of the LP_{01} mode, and the LP_{11a} mode has a larger resonance peak in the electrical field amplitude. As can be seen in Fig. 3(b) and (d), the penetration depths for the LP_{11a} and LP_{01} modes are 502 and 460 nm, respectively, which are much larger than the penetration depth of the SPR sensor in the visible wavelength.

We then investigate the impact of ITO film thickness on the sensing performance. The sensitivity S of the SPR sensor with spectral interrogation is defined as

$$S = \frac{\Delta\lambda_{res}}{\Delta n_e} \tag{1}$$

where $\Delta\lambda_{res}$ is the resonance wavelength shift and Δn_e is the change of n_e. The resonance wavelength and sensitivity of the sensor vary with the ITO film thickness. In order to obtain the optimized ITO film thickness, the film thickness is varied from 110 to 150 nm, with the residual fiber thickness fixed to 72 μm. The phase matching condition for coupling between the guided mode and the SP mode is changed when the ITO film thickness is varied. As shown in Fig. 4(a), the resonance wavelengths of the LP_{01} and LP_{11a} modes increase with ITO film thickness. In the thickness range from 110 to 150 nm, the resonance wavelengths of the LP_{01} and LP_{11a} modes change from 1475 to 1539 nm and from 1486 to 1546 nm with $n_e = 1.33$, respectively. In addition, the resonant wavelengths shift to longer wavelengths with n_e varied from 1.33 to 1.34. At an ITO film thickness of 150 nm, the resonant wavelengths shift from 1539 to 1598 nm and from 1546 to 1609 nm for the LP_{01} and LP_{11a} modes, respectively, when n_e is increased from 1.33 to 1.34. Note that resonant wavelengths of LP_{11a} mode locate at longer wavelengths compared with those of the LP_{01} mode. Fig. 4(b) shows the variation of sensitivity with ITO film thickness with n_e increased from 1.33 to 1.34. The sensitivity is the same for several values of ITO film thickness, which is caused by the 5-nm wavelength step used in our calculations. The sensitivity increases from 5628 to 5979 nm/RIU for the LP_{01} mode with the ITO film thickness varied from 110 to 150 nm. In comparison, the LP_{11a} mode has a higher sensitively, which increases from 5979 to 6332 nm/RIU in the same range of ITO film thickness.

Residual fiber thickness of the sensor has important effect on the sensing performance. The optimized d_{RFT} is obtained by varying it from 72 to 76 μm, with $d_{ITO} = 150$ nm. Similarly, variation of the residual fiber thickness results in changes of the phase matching condition. Fig. 5(a) depicts the resonance wavelength versus the residual fiber thickness. When d_{RFT} is changed from 72 to 76 μm, the resonance wavelengths of the LP_{01} and LP_{11a} modes increase from 1539 to 1569 nm and from 1546 to 1571 nm with $n_e = 1.33$, respectively. When n_e is varied from 1.33 to 1.34, the resonant wavelengths shift to longer wavelengths for both the LP_{01} and LP_{11a} modes. At a residual fiber thickness of 72 μm, the change of refractive index induces resonant wavelength shifts from

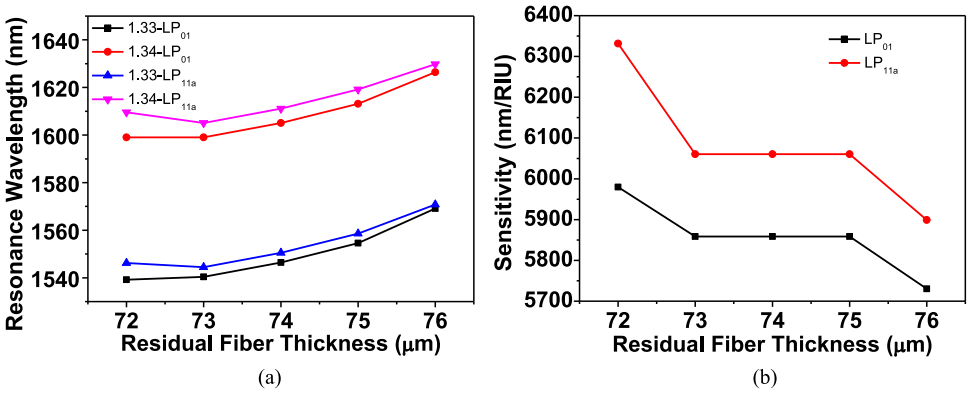

Fig. 5. (a) Resonant wavelength variation with residual fiber thickness with $d_{ITO} = 150$ nm and n_e varied from 1.33 to 1.34. (b) Sensitivity versus residual fiber thickness for LP_{01} and LP_{11a} modes with n_e increased from 1.33 to 1.34.

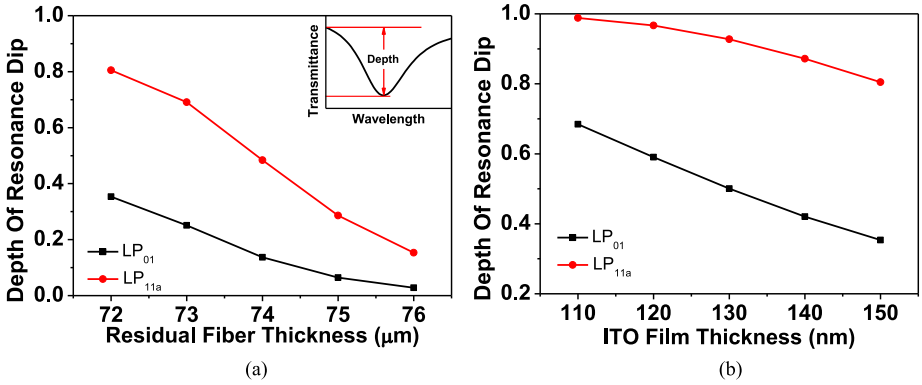

Fig. 6. (a) Depth of resonance dip versus residual fiber thickness, with $d_{ITO} = 150$ nm and $n_e = 1.34$. (b) Depth of resonance dip as a function of ITO film thickness, with $d_{RFT} = 72\,\mu$m and $n_e = 1.34$.

1539 to 1598 nm and from 1546 to 1609 nm for the LP_{01} and LP_{11a} modes, respectively. The LP_{11a} mode has a larger resonant wavelength than the LP_{01} mode. The sensitivity as a function of residual fiber thickness is plotted in Fig. 5(b). The sensitivity decreases from 5979 to 5730 nm/RIU and from 6332 to 5898 nm/RIU for the LP_{01} and LP_{11a} modes when d_{RFT} is increased from 72 to 76 μm, respectively. The largest sensitivity is obtained when the residual fiber thickness is 72 μm for both the LP_{01} and LP_{11a} modes, and the sensitivity of the LP_{11a} mode is higher than that of the LP_{01} mode. The ITO film is in direct contact with the core when the residual fiber thickness is 72 μm, which gives the largest evanescent filed.

3.2 Performance of the Sensor With Optimized Design

The optimized ITO film thickness and residual fiber thickness are 150 nm and 72 μm, respectively, which are used for the analysis of the sensing performance. The transmitted power of the sensor is calculated using the transmission function [37]:

$$T(\lambda) = \exp\left(-\frac{4\pi}{\lambda_0} imag\,(n_{eff})\,L\right) \tag{2}$$

where $T(\lambda)$ is the normalized transmission, λ_0 is wavelength of the light source, n_{eff} is the effective index of the SP mode, L is sensor length. The length of the sensor is 3 mm in the calculations. The resonance strength of the sensor is determined by the depth of resonance dip. Fig. 6(a) depicts the depth of resonance dip versus the residual fiber thickness with $d_{ITO} = 150$ nm and $n_e = 1.34$. The

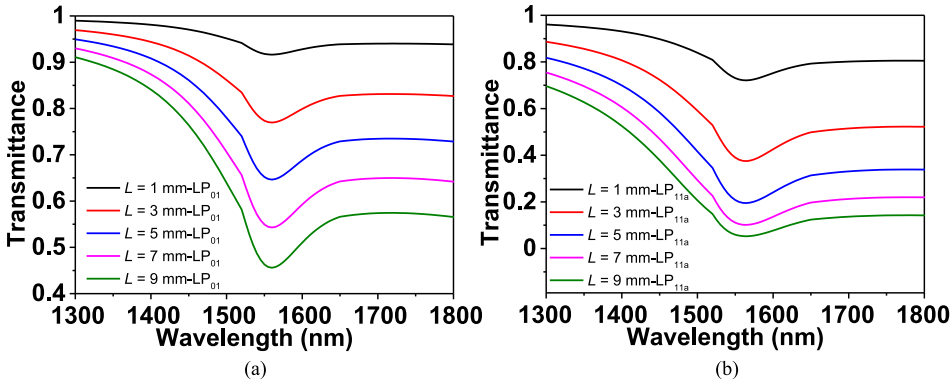

Fig. 7. Transmittance spectra with $n_e = 1.34$ when L is increased from 1 mm to 9 mm for (a) the LP_{01} mode and (b) the LP_{11a} mode.

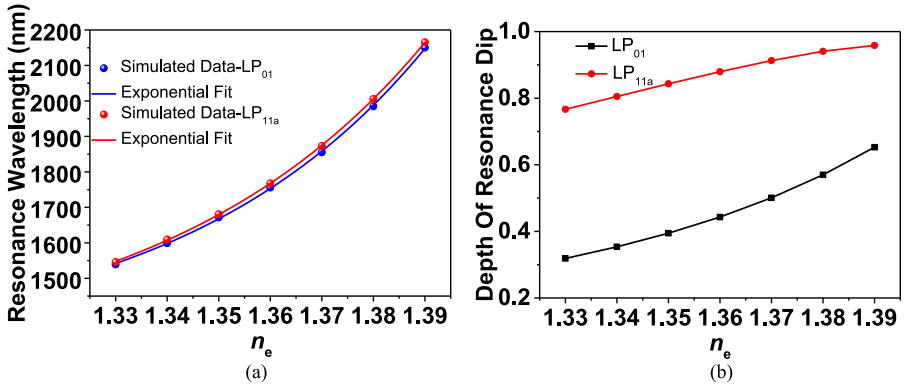

Fig. 8. (a) Numerical values of resonance wavelength as a function of n_e for the LP_{01} and LP_{11a} modes. (b) The depth of resonance dip as a function of n_e for the LP_{01} and LP_{11a} modes.

depth of resonance dip is defined in the inset of Fig. 6(a). The large residual fiber thickness leads to decreased depth of resonance dip for both the LP_{01} and LP_{11a} modes, indicating the resonance strength is reduced. The LP_{11a} mode has a larger depth of resonance dip than the LP_{01} mode. The dependence of depth of resonance dip on ITO film thickness is investigated. The thickness range from 110 to 150 nm is adopted taking into account the sensitivity and resonance wavelength. The depth of resonance dip decreases with the ITO film thickness for both the LP_{01} and LP_{11a} modes with $d_{RFT} = 72\,\mu$m and $n_e = 1.34$, as shown in Fig. 6(b). The depth of resonance dip of the LP_{11a} mode is larger than that of the LP_{01} mode.

The dependence of transmittance spectrum on sensor length is investigated with optimized ITO film thickness and residual fiber thickness. Fig. 7(a) and (b) show the transmittance spectra with L varied from 1 mm to 9 mm for the LP_{01} and LP_{11a} modes, respectively. The depth of resonance dip increases with the sensor length, but the transmittance spectrum becomes asymmetric and degenerate when the sensor length is increased.

Then, the performance of the sensor is analyzed by changing the refractive index of the analyte from 1.33 to 1.39. The dependence of resonance wavelength on the refractive index of the analyte is analyzed. As shown in Fig. 8(a), the resonance wavelength of the LP_{01} mode shifts from 1539 to 2148 nm for a change in n_e from 1.33 to 1.39, while for the LP_{11a} mode the shift in resonance wavelength is from 1546 to 2170 nm. The resonance wavelengths increase exponentially with increase in refractive index of analyte for both the LP_{01} and LP_{11a} modes. The average sensitivity for the n_e ranging from 1.33 to 1.39 is 10,149 and 10,400 nm/RIU for the LP_{01} and LP_{11a} modes, respectively. The sensor exhibits higher sensitivity for higher refractive index. In the n_e range from 1.38 to 1.39, the sensitivity reaches 16,355 and 16,453 nm/RIU for the LP_{01} and LP_{11a}

TABLE 1
Comparison of the Characteristics of Various Fiber SPR Sensors

Sensor Configuration	Detection Range (RIU)	Sensitivity (nm/RIU)	Wavelength Range (nm)
ITO coated TMF [This paper]	1.33–1.39	10,400	1300–2400
Gold nano-column coated SMF [38]	1.33–1.39	5,318	600–800
Gold film coated MMF [17]	1.33–1.40	4,989	600–800
Gold film coated PMF [22]	1.33–1.35	3,150	770–880
Gold film coated PCF [19]	1.32–1.36	3,186	600–800
Gold film coated PCF [22]	1.43–1.46	7,700	1100–1500

modes, respectively. Larger n_e gives rise to enhanced evanescent field, enabling sensing with higher sensitivity. Note that the LP_{11a} mode has higher sensitivity than the LP_{01} mode, this is because the LP_{11a} mode provides larger evanescent filed and subsequently enhances interaction of SP wave with the surrounding medium. The depth of resonance dip versus refractive index of the environment medium from 1.33 to 1.39 is shown in Fig. 8(b). Both the LP_{01} and LP_{11a} modes show an increase in the depth of resonance dip when the refractive index is increased, and the LP_{11a} mode has larger depths of resonance dip than the LP_{01} mode.

The sensitivity as well as the operating wavelength range for SPR sensors with various fiber architectures is tabulated in Table 1 for comparison. The sensitivity of the present sensor is much higher than the sensitivity of the gold-coated fiber sensors. In addition, the present sensor operates in the NIR. The higher sensitivity of the present sensor can be attributed to the ITO that allows sensor to be operated in NIR, because the larger penetration depth of the evanescent wave in NIR can enhance the interaction between the SP wave and the surrounding medium.

4. Conclusion

We have proposed and numerically investigated an SPR sensor based on side-polished TMF coated with ITO film. Results proved that the sensing performance of the sensor is influenced by the ITO film thickness and residual fiber thickness. Coupling between the LP_{11a} mode and an SP mode can achieve an average sensitivity of $\sim$10400 nm/RIU in the refractive index range from 1.33 to 1.39. The penetration depth of evanescent wave for the LP_{11a} is 502 nm. The sensitivity and penetration depth of the proposed sensor are larger than those of SMF and MMF based SPR sensors. This sensor can operate in the NIR region with high sensitivity and large penetration depth, which makes it promising for biological and chemical applications.

References

[1] J. Homola, S. S. Yee, and G. Gauglitz, "Surface plasmon resonance sensors: Review," *Sensors Actuators B. Chem.*, vol. 54, no. 1, pp. 3–15, 1999.
[2] A. K. Sharma, R. Jha, and B. D. Gupta, "Fiber-optic sensors based on surface plasmon resonance: A comprehensive review," *IEEE Sens. J.*, vol. 7, no. 8, pp. 1118–1129, Aug. 2007.
[3] S. Zeng, D. Baillargeat, H. P. Ho, and K. T. Yong, "Nanomaterials enhanced surface plasmon resonance for biological and chemical sensing applications," *Chem. Soc. Rev.*, vol. 43, no. 10, pp. 3426–3452, 2014.
[4] H. Moon, B. J. Sang, S. A. Kim, and S. J. Kim, "In vivo optical neural recording using fiber-based surface plasmon resonance," *Opt. Lett.*, vol. 37, no. 4, pp. 614–616, 2012.
[5] S. K. Mishra, S. N. Tripathi, V. Choudhary, and B. D. Gupta, "Surface plasmon resonance-based fiber optic methane gas sensor utilizing graphene-carbon nanotubes-poly(methyl methacrylate) hybrid nanocomposite," *Plasmonics*, vol. 10, no. 5, pp. 1147–1157, 2015.

[6] C. Caucheteur, V. Voisin, and J. Albert, "Near-infrared grating-assisted SPR optical fiber sensors: design rules for ultimate refractometric sensitivity," *Opt. Exp.*, vol. 23, no. 3, pp. 2918–2932, 2015.
[7] L. Coelho, J. M. M. M. D. Almeida, J. L. Santos, R. A. S. Ferreira, P. S. André, and D. Viegas, "Sensing structure based on surface plasmon resonance in chemically etched single mode optical fibres," *Plasmonics*, vol. 10, no. 2, pp. 319–327, 2015.
[8] J. Zhao *et al.*, "Surface plasmon resonance refractive sensor based on silver-coated side-polished fiber," *Sensors Actuators B, Chem.*, vol. 230, pp. 206–211, 2016.
[9] J. H. Ahn, T. Y. Seong, W. M. Kim, T. S. Lee, I. Kim, and K. S. Lee, "Fiber-optic waveguide coupled surface plasmon resonance sensor," *Opt. Exp.*, vol. 20, no. 19, pp. 21729–21738, 2012.
[10] S. F. Wang, M. H. Chiu, and R. S. Chang, "New idea for a D-type optical fiber sensor based on Kretschmann's configuration," *Opt. Eng.*, vol. 44, no. 3, 2005, Art. no. 030502.
[11] H. Y. Lin, C. H. Huang, G. L. Cheng, N. K. Chen, and H. C. Chui, "Tapered optical fiber sensor based on localized surface plasmon resonance," *Opt. Exp.*, vol. 20, no. 19, pp. 21693–21701, 2012.
[12] K. Takagi, H. Sasaki, A. Seki, and K. Watanabe, "Surface plasmon resonances of a curved hetero-core optical fiber sensor," *Sensors Actuators A, Phys.*, vol. 161, no. 1, pp. 1–5, 2010.
[13] Y. N. Kulchin, O. B. Vitrik, and A. V. Dyshlyuk, "Analysis of surface plasmon resonance in bent single-mode waveguides with metal-coated cladding by eigenmode expansion method," *Opt. Exp.*, vol. 22, no. 18, pp. 22196–22201, 2014.
[14] E. Klantsataya, P. Jia, H. Ebendorff-Heidepriem, T. Monro, and A. François, "Plasmonic fiber optic refractometric sensors: From conventional architectures to recent design trends," *Sensors*, vol. 17, no. 1, pp. 1–23, 2016.
[15] L. Coelho, J. M. M. M. de Almeida, J. L. Santos, R. A. S. Ferreira, P. S. André, and D. Viegas, "Sensing structure based on surface plasmon resonance in chemically etched single mode optical fibres," *Plasmonics*, vol. 10, no. 2, pp. 319–327, 2014.
[16] X. J. Feng *et al.*, "Design and optimization of surface plasmon resonance sensor based on side polished single-mode fiber," *Spectrosc. Spectr. Anal.*, vol. 35, no. 5, pp. 1419–1423, 2015.
[17] P. Mao *et al.*, "Design and optimization of surface plasmon resonance sensor based on multimode fiber," *Opt. Quant. Electron.*, vol. 47, no. 6, pp. 1–8, 2015.
[18] H. Suzuki, M. Sugimoto, Y. Matsui, and J. Kondoh, "Effects of gold film thickness on spectrum profile and sensitivity of a multimode-optical-fiber SPR sensor," *Sensors Actuators B, Chem.*, vol. 132, no. 1, pp. 26–33, 2008.
[19] Z. Tan, X. Li, Y. Chen, and P. Fan, "Improving the sensitivity of fiber surface plasmon resonance sensor by filling liquid in a hollow core photonic crystal fiber," *Plasmonics*, vol. 9, no. 1, pp. 167–173, 2014.
[20] J. N. Dash and R. Jha, "Highly sensitive side-polished birefringent PCF-Based SPR sensor in near IR," *Plasmonics*, vol. 11, no. 6, pp. 1505–1509, 2016.
[21] T. Huang, "Highly sensitive SPR sensor based on D-shaped photonic crystal fiber coated with indium tin oxide at near-infrared wavelength," *Plasmonics*, vol. 12, no. 3, pp. 583–588, 2017.
[22] R. K. Gangwar and V. K. Singh, "Highly sensitive surface plasmon resonance based D-shaped photonic crystal fiber refractive index sensor, *Plasmonics*, vol. 12, no. 5, pp. 1367–1372, 2017.
[23] Z. Fan *et al.*, "High-sensitivity of refractive index sensor based on analyte-filled photonic crystal fiber with surface plasmon resonance," *IEEE Photon. J.*, vol. 7, no. 3, Jun. 2015, Art. no. 4800809.
[24] M. Piliarik, J. Homola, Z. ManíKová, and J. Čtyroký, "Surface plasmon resonance sensor based on a single-mode polarization-maintaining optical fiber," *Sensors Actuators B, Chem.*, vol. 90, no. 1, pp. 236–242, 2003.
[25] Z. Liu *et al.*, "Twin-core fiber SPR sensor," *Opt. Lett.*, vol. 40, no. 12, pp. 2826–2829, 2015.
[26] H. S. Jang, K. N. Park, D. K. Chang, J. P. Kim, J. S. Sang, and K. S. Lee, "Optical fiber SPR biosensor with sandwich assay for the detection of prostate specific antigen," *Opt. Commun.*, vol. 282, no. 14, pp. 2827–2830, 2009.
[27] S. Franzen, "Surface plasmon polaritons and screened plasma absorption in indium tin oxide compared to silver and gold," *J. Phys. Chem. C*, vol. 112, no. 15, pp. 6027–6032, 2008.
[28] C. Rhodes *et al.*, "Surface plasmon resonance in conducting metal oxides," *J. Appl. Phys.*, vol. 100, no. 5, pp. 054905-1–054905-4, 2006.
[29] R. Ziblat, V. Lirtsman, D. Dan, and B. Aroeti, "Infrared surface plasmon resonance: A novel tool for real time sensing of variations in living cells," *Biophys. J.*, vol. 90, no. 7, pp. 2592–2599, 2006.
[30] G. G. Huang and J. Yang, "Development of infrared optical sensor for selective detection of tyrosine in biological fluids," *Biosensors Bioelectron.*, vol. 21, no. 3, pp. 408–418, 2005.
[31] Y. Wu *et al.*, "Graphene-based D-shaped fiber multicore mode interferometer for chemical gas sensing," *Opt. Lett.*, vol. 39, no. 20, pp. 6030–6033, 2014.
[32] B. C. Yao *et al.*, "Graphene based surface plasmonics in microfiber multimode interferometer for gas sensing," in *Proc. Adv. Photon.*, Barcelona, Spain, 2014, Paper SeW2C.4.
[33] S. K. Mishra, S. Rani, and B. D. Gupta, "Surface plasmon resonance based fiber optic hydrogen sulphide gas sensor utilizing nickel oxide doped ITO thin film," *Sensors Actuators B, Chem.*, vol. 195, pp. 215–222, 2014.
[34] R. K. Verma and B. D. Gupta, "Surface plasmon resonance based fiber optic sensor for the IR region using a conducting metal oxide film," *J. Opt. Soc. Amer. A*, vol. 27, no. 4, pp. 846–851, 2010.
[35] C. Rhodes *et al.*, "Dependence of plasmon polaritons on the thickness of indium tin oxide thin films," *J. Appl. Phys.*, vol. 103, no. 9, pp. 824–823, 2008.
[36] J. N. Dash and R. Jha, "SPR biosensor based on polymer PCF coated with conducting metal oxide," *IEEE Photon. Technol. Lett.*, vol. 26, no. 6, pp. 595–598, Mar. 2014.
[37] Y. Al-Qazwini, P. T. Arasu, and A. S. M. Noor, "Numerical investigation of the performance of an SPR-based optical fiber sensor in an aqueous environment using finite-difference time domain," in *Proc. 2nd Int. Conf. Photon.*, vol. 1, Kata Kinabalu, Malaysia, 2011, pp. 1–4.
[38] M. Yang *et al.*, "Design and optimization of nano-column array based surface plasmon resonance sensor," *Opt. Quant. Electron.*, vol. 49, no. 1, pp. 1–7, 2017.